

Phantom Higgs from Unparticles

A. Delgado^a, J. R. Espinosa^{b,c}, J. M. No^b and M. Quirós^d

^a*Department of Physics, 225 Nieuwland Science Hall, U. of Notre Dame,
Notre Dame, IN 46556-5670, USA*

^b*IFT-UAM/CSIC, Fac. Ciencias UAM, 28049 Madrid, Spain*

^c*CERN, Theory Division, CH-1211, Geneva 23, Switzerland*

^d*Institució Catalana de Recerca i Estudis Avançats (ICREA) at
IFAE, Universitat Autònoma de Barcelona, 08193 Bellaterra, Barcelona, Spain*

Abstract

A renormalizable coupling between the Higgs and a scalar unparticle operator \mathcal{O}_U of non-integer dimension $d_U < 2$ gives rise, after electroweak symmetry breaking, to a mass gap in the unparticle continuum and a shift in the original Higgs mass, which can end up above or below the mass gap. We show that, besides the displaced Higgs state, a new isolated state can generically appear in the spectrum near or below the mass gap. Such state (which we call phantom Higgs) is a mixture of Higgs and unparticles and therefore has universally reduced couplings to fermions and gauge bosons. This phenomenon could cause the mass of the lightest Higgs state accessible to colliders to be much smaller than the mass expected from the SM Lagrangian.

1 Introduction

It has been recently emphasized that the Standard Model (SM) Higgs boson can act as a privileged portal [1] to hidden sectors beyond the SM. For the case of hidden sectors made of unparticles [2] (i.e. conformally invariant sectors) this role of the Higgs boson has been explored in some detail in [3, 4]. More specifically one considers [5] the renormalizable coupling $\mathcal{O}_U|H|^2$ between a scalar operator of unparticles \mathcal{O}_U (of scaling dimension d_U , with $1 < d_U < 2$) and the SM Higgs field. As discussed in [3] such coupling induces a tadpole for \mathcal{O}_U after the breaking of the electroweak symmetry (inducing also the breaking of scale invariance in the unparticle sector [5]) and for $d_U < 2$ the value of the vacuum expectation value $\langle \mathcal{O}_U \rangle$ has an infrared (IR) divergence. This divergence can be easily cured by considering new interactions that induce an IR cutoff that makes $\langle \mathcal{O}_U \rangle$ finite: a simple additional interaction between the Higgs field and the unparticles was discussed in Ref. [3] while a quartic self-interaction among unparticles was instead considered in Ref. [4]. One of the main implications of such mechanisms was the appearance of a mass gap, m_g , of electroweak size for the unparticle sector above which the unparticle continuum extends¹. One expects such mass gap as a generic feature of any mechanism that solves the IR problem. Clearly, the existence of a mass gap has dramatic implications both for phenomenology and for constraints on the unparticle sector.

In addition, Ref. [3] showed that, after electroweak symmetry breaking (EWSB), the Higgs field mixes with the unparticle continuum above m_g in a way reminiscent of the Fano-Anderson model [7], familiar in solid-state and atomic physics as a description of the mixing between a localized state and a quasi-continuum. When the Higgs mass is below m_g , the Higgs survives as an isolated state but with some unparticle admixture that modifies its properties. On the other hand, the unparticle continuum above m_g gets a Higgs contamination which can be crucial to make it accessible experimentally. When the Higgs mass is above m_g the Higgs state gets subsumed into the unparticle continuum and the Higgs width gets greatly enlarged by the unparticle mixing. Such behaviour is similar to that found when the Higgs mixes with a quasi-continuum of graviscalars [8]. In both cases, with m_h above or below m_g , the properties of the mixed Higgs-unparticle system can be described quite neatly through a spectral function analysis.

In the case of the IR cure discussed in [4] one finds also unparticle resonances induced by the mixing with the Higgs and reminiscent of the plasmon excitations so common in condensed matter physics. In fact, the structure of the unparticle squared-mass matrix is similar to the Hamiltonian that describes different collective phenomena in several fields of physics [9].

The purpose of this paper is to revisit the IR cure proposed in [3]. We explore in more detail the available parameter space and find an additional interesting effect that was not discussed in [3]. When one starts with a Higgs interaction eigenstate well above the mass

¹The structure of an unparticle continuum above a mass gap has been related to a particular way of breaking scale invariance in the AdS/CFT context in [6].

gap, this original Higgs resonance gets shifted in mass due to unparticle mixing and gives rise to a broad Higgs state subsumed in the unparticle continuum and close to the original Higgs interaction eigenstate (as it was described above). However, if the Higgs-unparticle interaction is strong enough, in addition to the effect just described, an unexpectedly light isolated pole near or below the mass gap can appear. This pole is also a mixed Higgs-unparticle state which we call “phantom Higgs”, so that the spectrum can have two “Higgses” which are therefore experimentally accessible. However, their masses and widths (especially those of the phantom Higgs) are very different from the corresponding values for the SM Lagrangian.

We organize the paper as follows: in Section 2 we briefly review the stabilization mechanism for $\langle \mathcal{O}_U \rangle$ presented originally in [3]. In Section 3 we explore more thoroughly the rich parameter space available showing how the new effect mentioned above takes place. In Section 4 we perform an spectral function analysis which clarifies the structure of the spectrum in the new regime of interest and its phenomenological implications. We conclude in Section 5. The appendix contains an analytical proof of the correct normalization of the spectral function used in Section 4.

2 A Simple Solution to the Infrared Problem

We start with the following scalar potential

$$V_0 = m^2 |H|^2 + \lambda |H|^4 + \kappa_U |H|^2 \mathcal{O}_U , \quad (2.1)$$

where the first two terms are the usual SM Higgs potential and the last term is the Higgs-unparticle coupling (κ_U has mass dimension $2 - d_U$). As usual, the quartic coupling λ would be related in the SM to the Higgs mass at tree level by $m_{h_0}^2 = 2\lambda v^2$ (for $m^2 < 0$). We write the Higgs real direction as $Re(H^0) = (h^0 + v)/\sqrt{2}$, with $v = 246$ GeV.

The unparticle operator \mathcal{O}_U has dimension d_U , spin zero and its propagator is [2, 10]

$$P_U(p^2) = \frac{A_{d_U}}{2 \sin(\pi d_U)} \frac{i}{(-p^2 - i\epsilon)^{2-d_U}}, \quad A_{d_U} \equiv \frac{16\pi^{5/2}}{(2\pi)^{2d_U}} \frac{\Gamma(d_U + 1/2)}{\Gamma(d_U - 1)\Gamma(2d_U)} . \quad (2.2)$$

When the Higgs field gets a non zero vacuum expectation value (VEV) the scale invariance of the unparticle sector is broken [5]. From (2.1) we see that in such non-zero Higgs background the physical Higgs field mixes with the unparticle operator \mathcal{O}_U and also a tadpole appears for \mathcal{O}_U itself which will therefore develop a non-zero VEV.

As was done in Ref. [3], it is very convenient to use a deconstructed version of the unparticle sector, as proposed in [11]. One considers an infinite tower of scalars φ_n , ($n = 1, \dots, \infty$), with squared masses $M_n^2 = \Delta^2 n$. The mass parameter Δ is small and eventually taken to zero, limit in which one recovers a (scale invariant) continuous mass spectrum. As explained in [11], the deconstructed form of the operator \mathcal{O}_U is

$$\mathcal{O} \equiv \sum_n F_n \varphi_n , \quad (2.3)$$

where F_n is chosen as

$$F_n^2 = \frac{A_{d_U}}{2\pi} \Delta^2 (M_n^2)^{d_U-2} , \quad (2.4)$$

so that the two-point correlator of \mathcal{O} matches that of \mathcal{O}_U in the $\Delta \rightarrow 0$ limit. In the deconstructed theory then, the unparticle scalar potential, including the coupling (2.1) to the Higgs field, reads

$$\delta V = \frac{1}{2} \sum_n M_n^2 \varphi_n^2 + \kappa_U |H|^2 \sum_n F_n \varphi_n . \quad (2.5)$$

A non-zero VEV, $\langle |H|^2 \rangle = v^2/2$, triggers a VEV for the fields φ_n :

$$v_n \equiv \langle \varphi_n \rangle = -\frac{\kappa_U v^2}{2M_n^2} F_n , \quad (2.6)$$

thus implying, in the continuum limit,

$$\langle \mathcal{O}_U \rangle = -\frac{\kappa_U v^2}{2} \int_0^\infty \frac{F^2(M^2)}{M^2} dM^2 , \quad (2.7)$$

where

$$F^2(M^2) = \frac{A_{d_U}}{2\pi} (M^2)^{d_U-2} , \quad (2.8)$$

is the continuum version of (2.4). We see that $\langle \mathcal{O}_U \rangle$ has an IR divergence for $d_U < 2$, due to the fact that for $M \rightarrow 0$ the tadpole diverges while the mass itself, that should stabilize the unparticle VEV, goes to zero.

In Ref. [3] it was shown how one can easily get an IR regulator in (2.8) by including a coupling

$$\delta V = \zeta |H|^2 \sum_n \varphi_n^2 , \quad (2.9)$$

in the deconstructed theory. This coupling respects the conformal symmetry but will break it when H gets a VEV.

One can easily understand why (2.9) solves the IR problem in the continuum limit by defining the (dimensionless) field $u(x, M^2)$ by means of the redefinition $\varphi_n(x) = \Delta u_n(x)$ followed by $u(x, M^2) = \lim_{\Delta \rightarrow 0} u_n(x)$. In this way Eqs. (2.5) and (2.9) read as²

$$\delta V = \int_0^\infty dM^2 \left\{ \frac{1}{2} \left[M^2 + 2\zeta |H|^2 \right] u^2(x, M^2) + \kappa_U |H|^2 F(M^2) u(x, M^2) \right\} \quad (2.10)$$

²Concerning possible problems with locality, note that this term satisfies the cluster decomposition principle. In the continuum limit this can be shown after identifying the creation operator for unparticles with the appropriate integral in M^2 . In the deconstructed case, with a small but finite mass splitting, this principle is trivially satisfied.

In the absence of the term (2.9) the IR problem comes from the fact that the zero mode $u(x, 0)$ is massless. However in the presence of (2.9) the zero mode acquires a mass squared given by $2\zeta|H|^2$, which in the electroweak vacuum, where conformal invariance is broken, is given by ζv^2 . In this way the term (2.9) introduces an IR cutoff in the theory.

Now the vacuum expectation value $\langle \mathcal{O}_U \rangle$ becomes

$$\langle \mathcal{O}_U \rangle = -\frac{\kappa_U v^2}{2} \int_0^\infty \frac{F^2(M^2)}{M^2 + \zeta v^2} dM^2, \quad (2.11)$$

where we explicitly see the presence of a mass gap at

$$m_g^2 = \zeta v^2, \quad (2.12)$$

acting as an IR cutoff. The integral is now obviously finite for $1 < d_U < 2$ and reads explicitly

$$\langle \mathcal{O}_U \rangle = -\frac{1}{2} \kappa_U \frac{A_{d_U}}{2\pi} \zeta^{d_U-2} v^{2d_U-2} \Gamma(d_U - 1) \Gamma(2 - d_U). \quad (2.13)$$

Implications for EWSB of the coupling (2.9) were studied in Ref. [3].

3 Exploring the Parameter Space

In order to study the interplay between Higgs and unparticles we write down explicitly the infinite squared mass matrix that mixes the (real) neutral component h^0 of the Higgs with the deconstructed tower of unparticle scalars, φ_n . The different matrix elements are:

$$M_{hh}^2 = 2\lambda v^2 \equiv m_{h^0}^2, \quad (3.1)$$

$$M_{hn}^2 = \kappa_U v F_n \frac{M_n^2}{M_n^2 + m_g^2} \equiv A_n, \quad (3.2)$$

$$M_{nm}^2 = (M_n^2 + m_g^2) \delta_{nm}. \quad (3.3)$$

It is a simple matter to obtain the hh -entry of the inverse (infinite matrix) propagator associated to this infinite mass matrix. In the continuum limit we obtain:

$$iP_{hh}(p^2)^{-1} = p^2 - m_{h^0}^2 + J_2(p^2), \quad (3.4)$$

where [3]

$$\begin{aligned} J_2(p^2) &\equiv \int_0^\infty G_U(M^2, p^2) M^4 dM^2 = \frac{v^2}{p^4} (\mu_U^2)^{2-d_U} \Gamma(d_U - 1) \Gamma(2 - d_U) \\ &\times \left[(m_g^2 - p^2)^{d_U} + d_U p^2 (m_g^2)^{d_U-1} - (m_g^2)^{d_U} \right], \end{aligned} \quad (3.5)$$

with

$$G_U(M^2, p^2) \equiv \frac{v^2 (\mu_U^2/M^2)^{2-d_U}}{(M^2 + m_g^2 - p^2)(M^2 + m_g^2)^2}, \quad (3.6)$$

and

$$(\mu_U^2)^{2-d_U} \equiv \kappa_U^2 \frac{A_{d_U}}{2\pi} . \quad (3.7)$$

Due to the extra unparticle term in this propagator the Higgs pole will no longer be at its SM value $m_{h_0}^2$ but displaced from it. Whether this displacement is positive (towards higher masses) or negative will depend on the balance between two competing eigenvalue repulsion effects: the unparticle continuum above $m_{h_0}^2$ will tend to lower the Higgs mass while the continuum below will tend to increase it. Of course, when $m_{h_0}^2$ is below m_g^2 the shift is necessarily negative [3]. When the Higgs width is small so that one can neglect the imaginary part of the pole (complex in general) the final outcome for the Higgs pole at m_h^2 is well approximated by the solution to the pole equation

$$\mathcal{R}e \left[iP_{hh}(m_{hR}^2)^{-1} \right] = 0 , \quad (3.8)$$

where the subscript R indicates that m_{hR}^2 is the (real) pole of the real part of the propagator. As discussed in [3], the Higgs width can be greatly enlarged by unparticle mixing so that it is more appropriate to find the complex poles of the propagator:

$$P_{hh}(\tilde{m}_h^2)^{-1} = 0 , \quad (3.9)$$

with $\tilde{m}_h^2 \equiv m_h^2 - im_h\Gamma_h$, where m_h is the Higgs mass and Γ_h the (tree-level) Higgs width.

In order to explore the possible qualitative behaviours of the solutions to equation (3.9) it is convenient to express all squared masses in terms of the mass gap m_g^2 and of the dimensionless combination

$$R_U \equiv \frac{v^2}{m_g^2} \left(\frac{\mu_U^2}{m_g^2} \right)^{2-d_U} , \quad (3.10)$$

which measures the strength of the Higgs-unparticle interaction. The pole equation takes then the simple form

$$\tilde{x} = x_0 - \frac{R_U}{\tilde{x}^2} f_U(\tilde{x}) , \quad (3.11)$$

where

$$\tilde{x} \equiv \frac{\tilde{m}_h^2}{m_g^2} , \quad x_0 \equiv \frac{m_{h_0}^2}{m_g^2} , \quad (3.12)$$

and

$$f_U(\tilde{x}) = \Gamma(d_U - 1)\Gamma(2 - d_U) \left[(1 - \tilde{x})^{d_U} + d_U\tilde{x} - 1 \right] . \quad (3.13)$$

In order to solve the pole equation (3.11) one should specify in what Riemann sheet z^{d_U} is taken in (3.13). If one sticks to the principal sheet, with angles defined from $-\pi$ to

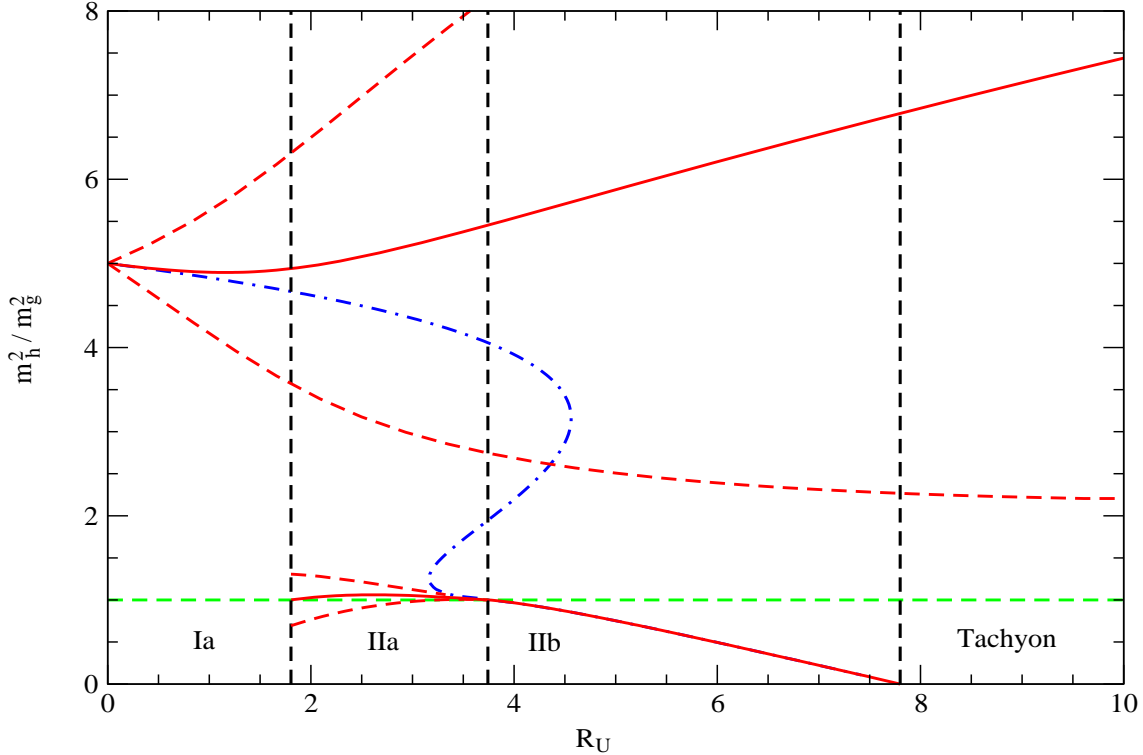


Figure 1: The solid red curves give the Higgs pole masses m_h^2 as a function of R_U for $m_{h0}^2 = 5m_g^2$ and $d_U = 1.2$ while the red-dashed curves give $m_h^2 \pm m_h \Gamma_h$. The dot-dashed blue line gives m_{hR} , the pole of the real part of the propagator. The horizontal dashed line gives m_g and the vertical dashed lines delimit the different zones as indicated by the labels.

π , the only possible poles appear in the real axis and below the mass gap. If one goes to the second Riemann sheet (with angles between -3π and $-\pi$) one finds also complex poles. We refer to these poles in the rest of the paper. The absence of complex poles in the principal sheet will be used with advantage in the appendix.

For small values of the unparticle effect, as measured by the parameter R_U (*i.e.* for $R_U \ll 1$), a perturbative solution gives

$$m_h^2 \simeq m_{h0}^2 - m_g^6 \frac{R_U}{m_{h0}^4} \mathcal{R}e[f_U(x_0)] , \quad (3.14)$$

with the sign of the shift determined by the sign of the function f_U [3] and

$$\Gamma_h \simeq m_g^6 \frac{R_U}{m_{h0}^5} \mathcal{I}m[f_U(x_0)] \theta(x_0 - 1) . \quad (3.15)$$

Although the analysis of [3] was not restricted to very small values of R_U , the behaviour of m_h^2 discussed there was qualitatively similar to the one just described.

New interesting effects occur when larger values of R_U are probed. Fig. 1 illustrates this for the particular case $d_U = 1.2$ and $m_{h0}^2/m_g^2 = 5$ by showing m_h^2 (solid lines) as a

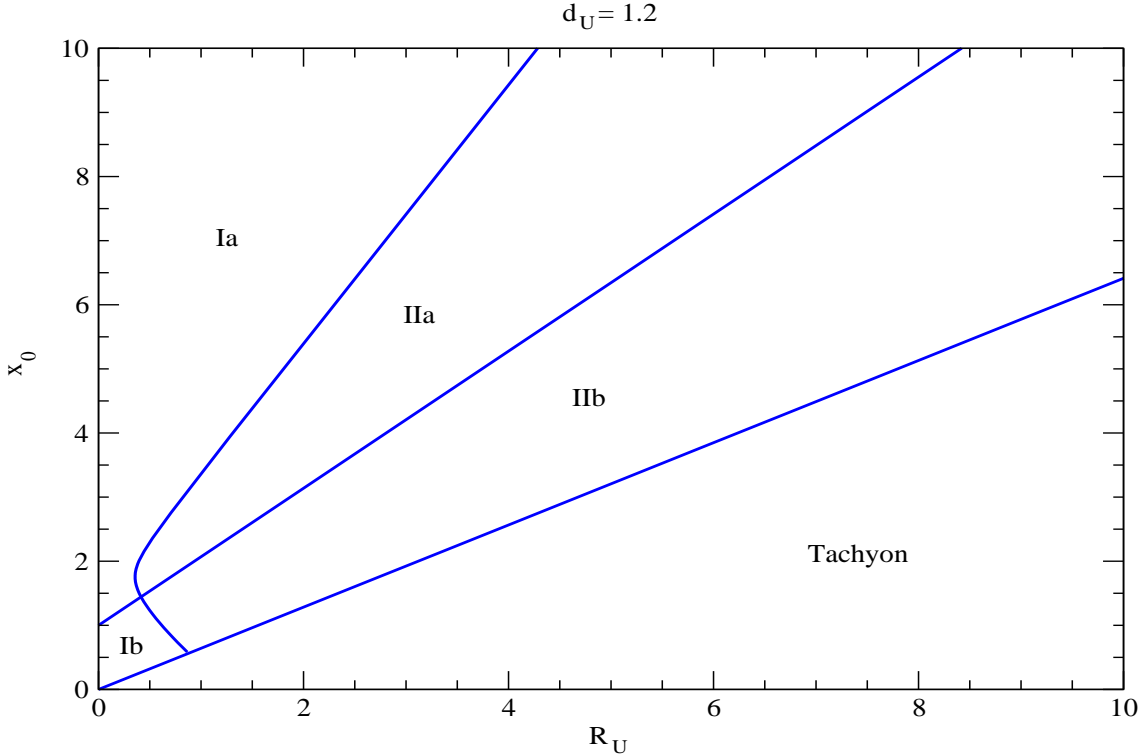


Figure 2: Different zones in the plane $(R_U, x_0 = m_{h0}^2/m_g^2)$ with different number of Higgs poles: one in zone I (above m_g in zone Ia, below in zone Ib) and two in zone II (both above m_g in IIa, one above and one below in IIb). In the zone labeled “Tachyon” the lightest pole becomes tachyonic.

function of R_U . For small R_U one simply gets a negative shift for m_h (zone marked as Ia). However, for larger values of R_U ($R_U \gtrsim 1.8$) things get much more interesting. In zone IIa one finds two Higgs poles above m_g , one of them very close to the mass gap and the other closer to the initial value m_{h0} . In zone IIb the lighter of these poles, the phantom Higgs, goes below the mass gap while the other gets heavier. Eventually, for sufficiently large R_U , the squared mass of the phantom pole gets negative and the state becomes tachyonic. We also show the width of these poles by giving (dashed lines) the curves for $m_h^2 \pm m_h \Gamma_h$ (we come back to the discussion of this width in section 4, using the spectral function technique). We see that the heavy pole gets wider and wider with increasing R_U while the lighter has always a small width. When the light Higgs gets below the mass gap its width (at tree-level) is zero. For comparison, we also show in this figure the value of m_{hR} (dot-dashed line). We see that it approximates well m_h when the Higgs width is small but can be very different from it when the width gets larger.

Zone II is particularly striking: the initial SM Higgs pole, which was well above the mass gap into the unparticle continuum, gets swallowed up by this continuum which spits out a much lighter pole near (IIa) or below (IIb) the mass gap. A similar phenomenon has been described in other fields of physics, see *e.g.* [12]. This behaviour is generic and

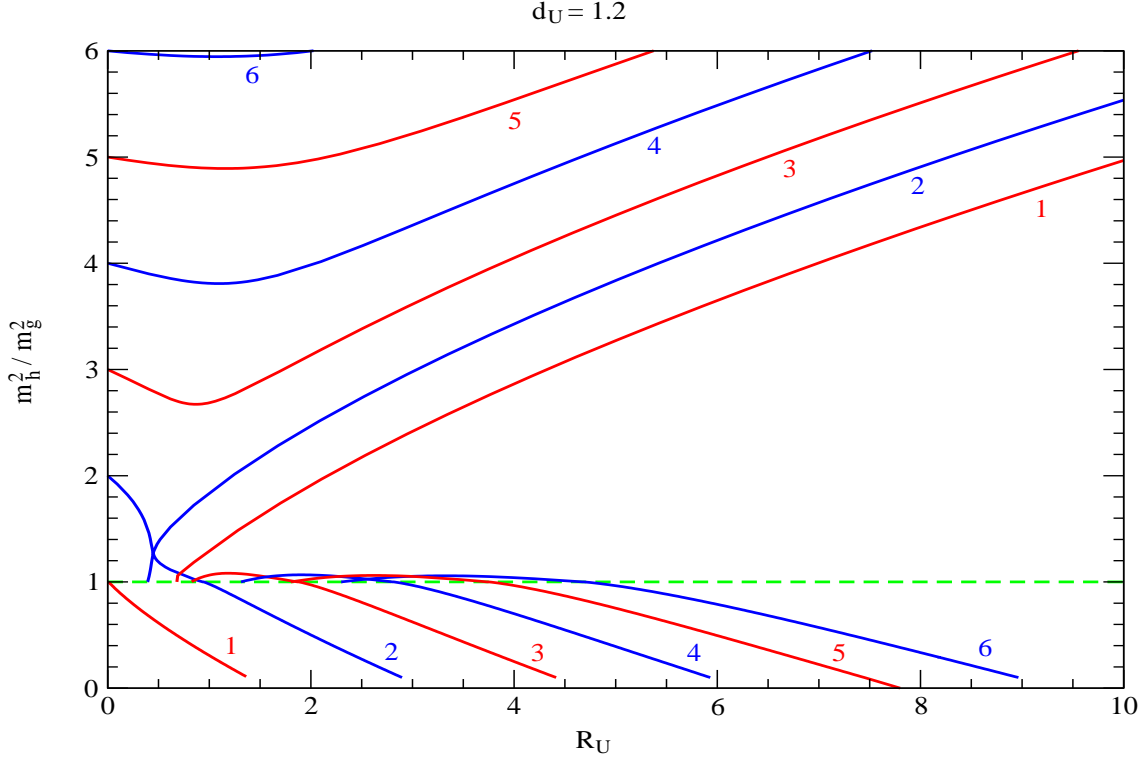


Figure 3: Same as Fig. 1 for different values of $x_0 = m_{h_0}^2/m_g^2$ as indicated by the labels.

persists for other values of $x_0 = m_{h_0}^2/m_g^2$ and/or d_U . Fig. 2 shows the different zones, with the same coding as explained above, in the plane (x_0, R_U) for $d_U = 1.2$. In addition to the zones discussed above, there is also the possibility of having a single pole below the mass gap, corresponding to zone Ib in this plot. We do not give contour lines of $x = m_h^2/m_g^2$ as they would overlap in regions with two poles, making the figure clumsy. Between the lines delimiting zone Ib+IIb the mass of the pole below m_g tends to zero at the lower boundary (the border with the tachyonic zone) and to m_g in the upper boundary. In the boundary between zones Ia and IIa the mass of the light Higgs is also m_g .

Fig. 3 shows m_h^2 vs. R_U for different values of the initial x_0 . The case corresponding to $x_0 = 1$ displays, for small R_U , the behaviour associated to zone Ib, with a single pole below the mass gap. For larger R_U , however, we see that an additional pole appears above the mass gap. Notice that (in all cases) once the lighter phantom Higgs becomes tachyonic the parameter choice is not acceptable. To answer the question of which pole carries a higher Higgs composition one can use a spectral function analysis as discussed in the next section.

4 Spectral Function Analysis

To clarify the pole structure of the mixed Higgs-unparticle propagator we now turn to the study of its spectral function, given by

$$\rho_{hh}(s) = -\frac{1}{\pi} \text{Im}[-iP_{hh}(s+i\epsilon)] , \quad (4.1)$$

where the limit $\epsilon \rightarrow 0$ is understood. We can calculate easily this spectral function by using $1/(x+i\epsilon) \rightarrow \text{P.V.}[1/x] - i\pi\delta(x)$ directly in the integral J_2 of (3.5) to obtain, for $s > m_g^2$,

$$J_2(s+i\epsilon) = R_2(s) + iI_2(s) , \quad (4.2)$$

with

$$\begin{aligned} R_2(s) &= \text{P.V.}[J_2(s)] , \\ I_2(s) &= \pi \frac{v^2}{s^2} (\mu_U^2)^{2-d_U} (s - m_g^2)^{d_U} . \end{aligned} \quad (4.3)$$

When there is one pole below the mass gap, and irrespective of whether there is another pole above it or not, the spectral function takes the form [3]

$$\rho_{hh}(s) = \frac{1}{K^2(m_h^2)} \delta(s - m_h^2) + \theta(s - m_g^2) \frac{T_U(s)}{\mathcal{D}^2(s) + \pi^2 T_U^2(s)} , \quad (4.4)$$

where $\mathcal{D}(s)$ and $\pi T_U(s)$ are the real and imaginary parts of $iP_{hh}(s+i\epsilon)^{-1}$ when $s > m_g^2$:

$$iP_{hh}(s+i\epsilon)^{-1} = \mathcal{D}(s) + i\pi T_U(s) = [s - m_{h0}^2 + R_2(s)] + iI_2(s) . \quad (4.5)$$

Finally,

$$K^2(s_0) \equiv \left. \frac{d}{ds} \mathcal{D}(s) \right|_{s=s_0} . \quad (4.6)$$

An explicit expression for $K^2(m_h^2)$ can be obtained directly from $\mathcal{D}(s)$ above. When all the poles are above m_g the spectral function is given by the same continuum function as in (4.4) without the Dirac-delta term.

One can check (see appendix for an analytical proof) that the spectral function (4.4) is properly normalized:

$$\int_0^\infty \rho_{hh}(s) ds = 1 . \quad (4.7)$$

The physical interpretation of this spectral function was discussed in [4]: Calling $|h\rangle$ the Higgs interaction eigenstate and $|u, M\rangle$ the unparticle interaction eigenstates (a continuous function of M) and $|H\rangle$, $|U, M\rangle$ the respective mass eigenstates after EWSB, with $|H\rangle$

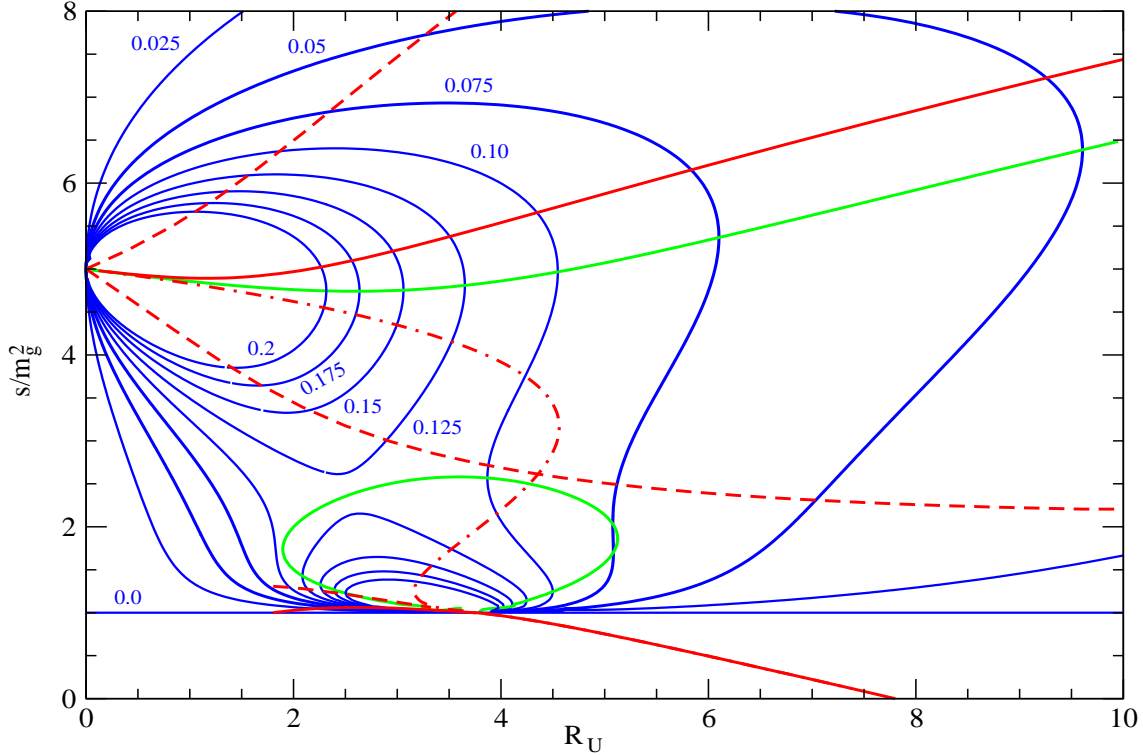


Figure 4: Contour lines of $\rho_{hh}(s)$ (we stop at 0.2) in the plane $(R_U, s/m_g^2)$ for $d_U = 1.2$, $x_0 = 5$ (blue lines). Information on the Higgs poles is given by the same curves as in Fig. 1. The green lines give the extrema of the spectral function at fixed R_U .

being the isolated state below the mass gap (we consider this particular case to illustrate the interpretation), one has

$$\rho_{hh}(s) \equiv \langle h|s\rangle\langle s|h\rangle = |\langle H|h\rangle|^2\delta(s - m_h^2) + \theta(s - m_g^2)|\langle U, M|h\rangle|^2, \quad (4.8)$$

so that one can read-off the Higgs composition of the isolated pole and the unparticle continuum directly from (4.4). The proper normalization (4.7) is simply a consequence of the proper normalization of $|h\rangle$, *i.e.* $|\langle h|h\rangle|^2 = 1$. The amount of $|h\rangle$ admixture in any state is an important quantity because it determines key properties of that state, like its coupling to gauge bosons, that are crucial for its production and decay.

In Figs. 4 and 5 we show the spectral function for the case $d_U = 1.2$, $x_0 = 5$ and varying R_U . In Fig. 4 we give contour lines of $\rho_{hh}(s)$ (we stop them at 0.2) in the plane $(R_U, s/m_g^2)$. We see two global peaks above the mass gap, one is at $(R_U = 0, s/m_g^2 = x_0)$, corresponding to the SM Higgs resonance, and the other at $(R_U \simeq 3.5, s/m_g^2 = 1)$ corresponding to the phantom Higgs. For $R_U \gtrsim 3.5$ this phantom Higgs drops below the mass gap giving rise to a delta pole in the spectral function. We show by the solid red lines the Higgs poles in this particular case (corresponding to Fig. 1). The green solid lines give the extrema of the spectral function for fixed R_U . We see that the pole lines offer reliable information

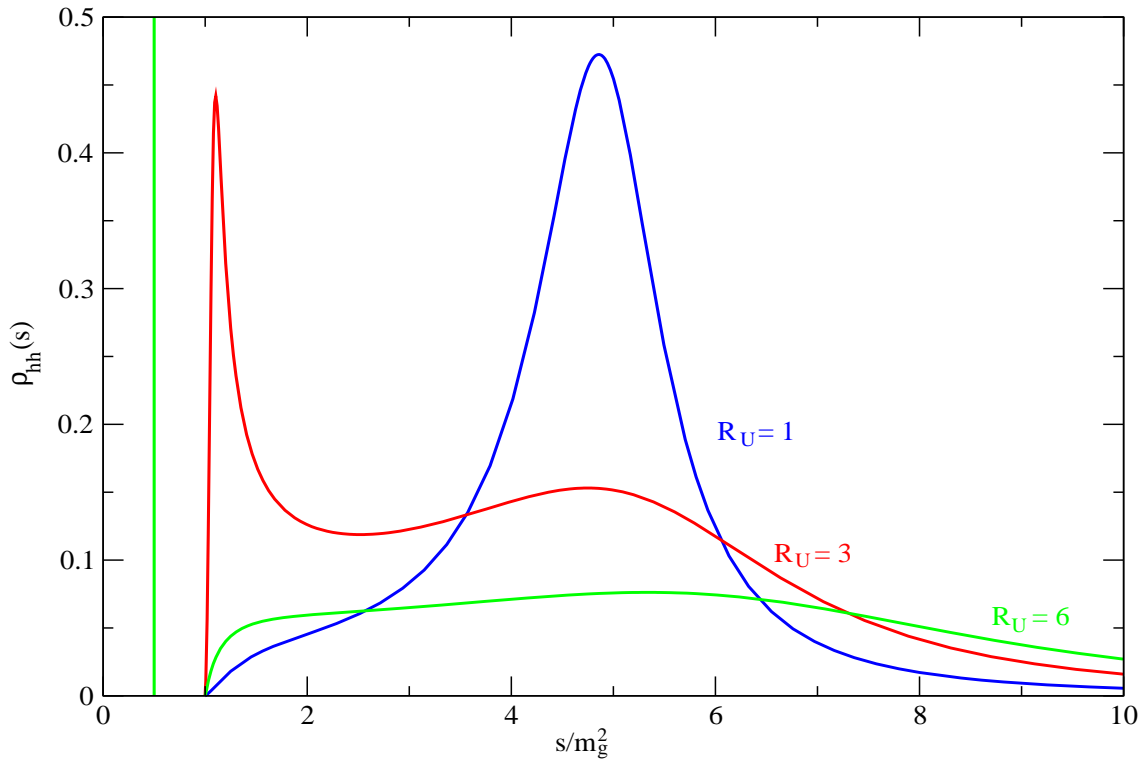


Figure 5: Cuts of Fig. 4 along fixed R_U values, as indicated.

about the location of the maxima of the spectral function (we should not expect perfect correspondence, see *e.g.* [13]) and their widths while the dashed curve corresponding to m_{hR} is only a good approximation near the global peaks and along the isolated pole (where the tree-level Higgs width is small or zero). In any case, it is clear that the spectral function carries more information concerning the structure of the Higgs propagator than simply giving the location and width of its poles and it is therefore much more useful to deal directly with it. To clarify even further the structure of the spectral function, Fig. 5 gives $\rho_{hh}(s)$ at various fixed values of R_U for the same parameters as before, $d_U = 1.2$ and $x_0 = 5$. For $R_U = 1$ there is only one pole, it is above m_g and corresponds to the somewhat wide resonance of the spectral function (zone Ia). One can directly relate the width of this resonance (as measured by the width across it at half the peak maximum) with the width as given by the dashed lines in Fig. 1. For $R_U = 3$, the pole above m_g has become wider and less pronounced while a sharper resonance has appeared right above the mass gap (zone IIa). Notice that the continuum part of the spectral function does not extend below the gap. This is in contrast with the behaviour of the complex pole near m_g shown in Fig. 1: from there, after taking into account the width, one would conclude that the light resonance extends below m_g . For $R_U = 6$ this resonance has detached from the continuum giving a delta function below m_g . The pole above m_g is very broad and shallow (zone IIb) and could hardly be called a resonance.

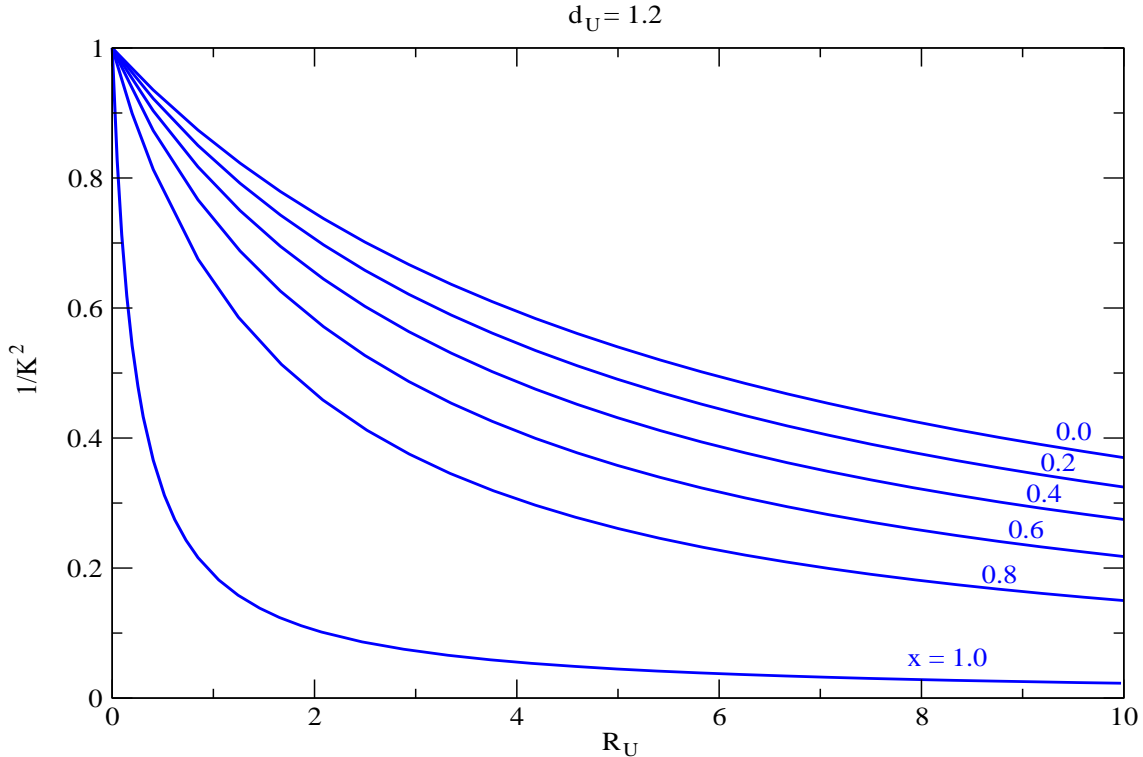


Figure 6: Pure Higgs composition of the isolated pole below m_g as a function of R_U for different values of $x = m_h^2/m_g^2$ and for $d_U = 1.2$.

From the previous figures one cannot obtain information on the prefactor $1/K^2$ which weights the Dirac delta contribution to $\rho_{hh}(s)$ when there is a pole below m_g and gives information of the pure Higgs composition of that pole, as explained above. This information is given by Fig. 6 (valid for $d_U = 1.2$), where the different lines correspond to different values of $x = m_h^2/m_g^2$ from $x = 0$ to $x \rightarrow 1^-$. When the influence of unparticles is small (small R_U) $1/K^2 \rightarrow 1$ as it should be for a Higgs with SM properties. The departure of $1/K^2$ from 1 is larger for larger R_U (larger unparticle mixing) or when m_h gets closer to m_g (smaller mass difference between the states that mix).

5 Conclusions

The Standard Model Higgs boson offers a unique opportunity to probe the scalar part of an unparticle sector through a direct renormalizable coupling of the form $|H|^2\mathcal{O}_U$, where \mathcal{O}_U is an unparticle scalar operator of non-integer dimension d_U , with $1 < d_U < 2$. Several interesting effects follow from such a coupling after electroweak symmetry breaking, both for unparticle phenomenology and for Higgs boson properties, as has been discussed recently in [5, 3, 4]. Among these effects we have: a mass gap m_g of electroweak size is generated above which lies the unparticle continuum (which therefore does not extend

all the way to zero mass). This unparticle continuum mixes with the Higgs so that the Higgs resonance gets some unparticle admixture that changes the Higgs couplings from its SM values while the Higgs admixture of the unparticle continuum helps in making it accessible experimentally. The Higgs mass is also affected by the unparticle mixing getting shifted from its SM value. If it ends above the mass gap it gets subsumed in the unparticle continuum and becomes very wide at tree-level due to such mixing.

In this paper we have found yet another remarkable effect: starting with a SM Higgs mass well above the unparticle mass gap, into the continuum, if the Higgs-unparticle interaction is large enough, a “phantom” Higgs besides the original one will appear near or below the mass gap. It will have some unparticle admixture and some Higgs composition that makes it, in principle, accessible experimentally. Therefore the spectrum will contain two Higgs resonances: one heavy and wide, clearly related to the original SM Higgs state and another thin and much lighter than one would naively expect from the parameters of the SM part of the potential.

Acknowledgments

J.R.E. thanks CERN for hospitality and partial financial support. J.M.N. thanks IFAE, Barcelona, for hospitality. Work supported in part by the European Commission under the European Union through the Marie Curie Research and Training Networks “Quest for Unification” (MRTN-CT-2004-503369) and “UniverseNet” (MRTN-CT-2006-035863); by the Spanish Consolider-Ingenio 2010 Programme CPAN (CSD2007-00042); by a Comunidad de Madrid project (P-ESP-00346) and by CICYT, Spain, under contracts FPA 2007-60252 and FPA 2005-02211.

Appendix A

In this appendix we give an analytical proof of the normalization condition (4.7) for the spectral function used in section 4. The proof uses complex integration methods very common in the literature of dispersion techniques. Take the hh -propagator of Eqs. (3.4-3.5) to be defined in the complex plane, $P_{hh}(z)$, and integrate it along the contour of Fig. 7, which shows the general case with a real pole below the mass gap and a branch cut from that mass gap to infinity. The absence of complex poles of $P_{hh}(z)$ in the principal branch (see discussion in Section 3) tells us that

$$\oint_C P_{hh}(z) dz = 0 . \tag{A.1}$$

Along the circle at infinity, with $z = Re^{i\theta}$, noting that $P_{hh} \sim 1/(Re^{i\theta})$ we get a constant contribution:

$$\oint_{C_\infty} P_{hh}(z) dz \simeq \int_0^{2\pi} \frac{iRe^{i\theta} d\theta}{Re^{i\theta}} = 2i\pi . \tag{A.2}$$

The integral along the real axis is

$$\oint_{C_{pole}} P_{hh}(z) dz + \int_{m_g^2}^{\infty} ds [P_{hh}(s + i\epsilon) - P_{hh}(s - i\epsilon)] , \quad (\text{A.3})$$

where C_{pole} is an infinitesimal contour encircling clockwise the real pole (at $z = m_h^2$). The integral around this pole is evaluated using the theorem of residues and gives

$$\oint_{C_{pole}} P_{hh}(z) dz = -2i\pi \left. \frac{1}{\mathcal{D}'(s)} \right|_{s=m_h^2} = -2i\pi \frac{1}{K^2(m_h^2)} , \quad (\text{A.4})$$

so that one can also write

$$\oint_{C_{pole}} P_{hh}(z) dz = -2i\pi \int_0^{m_g^2} \frac{1}{K^2(s)} \delta(s - m_h^2) ds = -2i\pi \int_0^{m_g^2} \rho_{hh}(s) ds . \quad (\text{A.5})$$

For the second piece in (A.3) we use (4.1) to write $P_{hh}(s + i\epsilon) = -i\pi\rho_{hh}(s)$. Then, notice that for this particular $P_{hh}(z)$ we also have (this is not always the case) $P_{hh}(s - i\epsilon) = i\pi\rho_{hh}(s)$. Putting all pieces together, (A.1) leads to

$$\int_0^{\infty} \rho_{hh}(s) ds = 1 . \quad (\text{A.6})$$

This is the correct normalization of the spectral function for a stable state.

References

- [1] B. Patt and F. Wilczek, [hep-ph/0605188].
- [2] H. Georgi, Phys. Rev. Lett. **98** (2007) 221601 [hep-ph/0703260]; Phys. Lett. B **650** (2007) 275 [hep-ph/0704.2457].
- [3] A. Delgado, J. R. Espinosa and M. Quirós, JHEP **0710** (2007) 094 [hep-ph/0707.4309].
- [4] A. Delgado, J. R. Espinosa, J. M. No and M. Quirós, [hep-ph/0802.2680].
- [5] P. J. Fox, A. Rajaraman and Y. Shirman, Phys. Rev. D **76** (2007) 075004 [hep-ph/0705.3092]; M. Bander, J. L. Feng, A. Rajaraman and Y. Shirman, Phys. Rev. D **76** (2007) 115002 [hep-ph/0706.2677]; G. Cacciapaglia, G. Marandella and J. Terning, JHEP **0801** (2008) 070 [hep-ph/0708.0005].
- [6] G. Cacciapaglia, G. Marandella and J. Terning, [hep-ph/0804.0424].
- [7] P.W. Anderson, Phys. Rev. **124** (1961) 41; U. Fano, Phys. Rev. **124** (1961) 1866; G.D. Mahan, *Many-Particle Physics*, Plenum Press, New York, 1990.
- [8] G. F. Giudice, R. Rattazzi and J. D. Wells, Nucl. Phys. B **595** (2001) 250 [hep-ph/0002178].

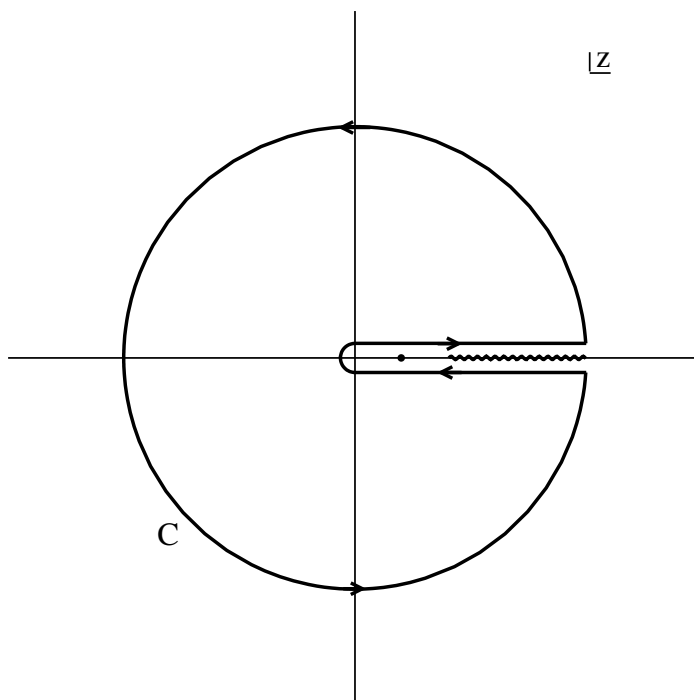


Figure 7: Integration contour for $P_{hh}(z)$ in the complex z -plane.

- [9] U. Fano, Rev. Mod. Phys. **64** (1992) 313.
- [10] K. Cheung, W. Y. Keung and T. C. Yuan, Phys. Rev. Lett. **99** (2007) 051803 [hep-ph/0704.2588].
- [11] M. A. Stephanov, Phys. Rev. D **76** (2007) 035008 [hep-ph/0705.3049]; N. V. Krasnikov, Int. J. Mod. Phys. A **22** (2007) 5117 [hep-ph/0707.1419].
- [12] B. Gaveau and L.S. Schulman, J. Phys. A: Math. Gen. **28** (1995) 7359.
- [13] L. Jahnke and S. Leupold, Nucl. Phys. A **778** (2006) 53 [nucl-th/0601072].